



# AMERICAN METEOROLOGICAL SOCIETY

*Journal of Atmospheric and Oceanic Technology*

## **EARLY ONLINE RELEASE**

This is a preliminary PDF of the author-produced manuscript that has been peer-reviewed and accepted for publication. Since it is being posted so soon after acceptance, it has not yet been copyedited, formatted, or processed by AMS Publications. This preliminary version of the manuscript may be downloaded, distributed, and cited, but please be aware that there will be visual differences and possibly some content differences between this version and the final published version.

The DOI for this manuscript is doi: [10.1175/JTECH-D-10-05044.1](https://doi.org/10.1175/JTECH-D-10-05044.1)

The final published version of this manuscript will replace the preliminary version at the above DOI once it is available.



**Development and application of a compact, tunable, solid-state airborne ozone lidar system for boundary layer profiling**

R. J. Alvarez II<sup>1</sup>, C. J. Senff<sup>1,2</sup>, A. O. Langford<sup>1</sup>, A. M. Weickmann<sup>1,2</sup>, D. C. Law<sup>1</sup>, J. L. Machol<sup>1,2,3</sup>, D. A. Merritt<sup>1,4</sup>, R. D. Marchbanks<sup>1,2</sup>, S. P. Sandberg<sup>1</sup>, W. A. Brewer<sup>1</sup>, R. M. Hardesty<sup>1</sup>, R. M. Banta<sup>1</sup>

<sup>1</sup>NOAA Earth System Research Laboratory, Chemical Sciences Division, Boulder, CO 80305, USA

<sup>2</sup>Cooperative Institute for Research in Environmental Sciences, University of Colorado and NOAA Earth System Research Laboratory, Chemical Sciences Division, Boulder, CO 80305, USA

<sup>3</sup>Currently with Cooperative Institute for Research in the Atmosphere, Colorado State University and NOAA Space Weather Prediction Center, Boulder, CO 80305, USA

<sup>4</sup>Contract with Science & Technology Corporation, Hampton, VA 23666, USA

Submitted to *J. Atmos. Oceanic Technol.*

December 8, 2010

Revised April 12, 2011

Corresponding author: Raul J. Alvarez II, NOAA Earth System Research Laboratory, 325 Broadway, R/CSD3, Boulder, CO 80305, USA. (Raul.Alvarez@noaa.gov)

## **Abstract**

The Chemical Sciences Division of the National Oceanic and Atmospheric Administration Earth System Research Laboratory (NOAA/ESRL/CSD) has developed a versatile, airborne lidar system for measurement of ozone and aerosols in the boundary layer and lower free troposphere. The Tunable Optical Profiler for Aerosol and oZone (TOPAZ) lidar was deployed aboard a NOAA Twin Otter aircraft during the Texas Air Quality Study (TexAQS 2006) and the California Research at the Nexus of Air Quality and Climate Change (CalNex 2010) field campaigns. TOPAZ is capable of measuring ozone concentrations in the lower troposphere with uncertainties of several ppbv at 90 m vertical and 600 m horizontal resolution from an aircraft flying at 60 m s<sup>-1</sup>. The system also provides uncalibrated aerosol backscatter profiles at 18 m vertical and 600 m horizontal resolution. TOPAZ incorporates state-of-the-art technologies, including a cerium-doped lithium calcium aluminum fluoride (Ce:LiCAF) laser, to make it compact and lightweight with low power consumption. The tunable, 3-wavelength UV laser source makes it possible to optimize the wavelengths for differing atmospheric conditions, reduce the interference from other atmospheric constituents, and implement advanced analysis techniques. This paper describes the TOPAZ lidar, its components, performance during testing and field operation, and the data analysis procedure including a discussion of error sources. The performance characteristics are illustrated through a comparison between TOPAZ and an ozonesonde launched during the TexAQS 2006 field campaign. A more comprehensive set of comparisons with in situ measurements during TexAQS 2006 and an assessment of the TOPAZ accuracy and precision are presented in a companion paper.

## **1. Introduction**

The formation and transport of ozone and aerosol pollution in the lower troposphere is of great interest because of the negative impacts these pollutants have on both air quality and climate (the Royal Society, 2008 and references therein). These processes have been studied extensively over the last several decades, with numerous field studies aimed at providing detailed measurements of the ozone and aerosol distribution in and around large urban areas where many of the photochemical precursors of these pollutants are emitted. In many of these studies, airborne lidar systems have played a key role by providing highly resolved measurements of the 3-dimensional distribution of ozone and aerosols. Several research groups have built and deployed lidar systems for airborne detection of ozone using a variety of transmitter and receiver designs. These systems are based on the differential absorption lidar (DIAL) technique (Schotland 1974), and generally fall into two design classes. The first approach, pioneered by the NASA Langley Research Center (e.g. Browell et al. 1983), uses high power tunable dye lasers for the lidar transmitter. The resulting system is extremely versatile, but is relatively large with high power consumption and thus is restricted to large aircraft platforms that are costly to operate. The second approach, which uses fixed wavelength lasers (e.g. Uthe et al 1992; Alvarez et al. 1998; Ancellet and Ravetta 1998), can be made more compact for operation on smaller aircraft, but cannot be optimized (Proffitt and Langford 1997) to maximize the spatial and temporal resolution and minimize unwanted interferences.

Recent developments in tunable UV solid-state laser technology (Coutts and McGonigle 2004) have bridged the gap between these two approaches (Elsayed et al. 2002; Fix et al. 2002; Prasad et al. 2006, Rambaldi et al. 1995). Building upon the NOAA Earth System Research Laboratory's experience with ground-based and airborne tropospheric ozone lidars (Machol et al. 2009; Alvarez et al. 1998), we have designed and built the Tunable Optical Profiler for Aerosol and oZone (TOPAZ) lidar (Alvarez et al. 2008), a new airborne lidar system for measurements of ozone and aerosol backscatter in the lower troposphere. This system incorporates recent advances in state-of-the-art lasers and computers resulting in a more compact and lighter lidar with lower power requirements that can be deployed on smaller aircraft platforms including the NOAA Twin Otter. TOPAZ uses a laser with high pulse rates and low pulse energy to permit eye-safe operation with short integration times while airborne. This tunable, 3-wavelength UV laser provides TOPAZ with significantly enhanced capabilities including the optimization of wavelengths for differing atmospheric conditions, the reduction of interference from other atmospheric constituents, and the option to use the dual-DIAL technique to measure ozone concentration profiles.

## **2. Lidar description**

TOPAZ (Figure 1) is an airborne, nadir-viewing, 3-wavelength DIAL system. It provides ozone and aerosol backscatter profiles from approximately 400 m below the aircraft to near ground level (flights are typically conducted at altitudes ranging from 3000 to 5000 m above mean sea level (MSL)). Profiles are acquired continuously at 10 s intervals providing a 2-dimensional "curtain" measurement of ozone and aerosol

backscatter as the aircraft moves along the flight path. These curtain plots can be combined to show the 3-dimensional structure or time evolution of the ozone and aerosol distribution. During flights, a real-time display allows the operators to monitor preliminary ozone and aerosol profiles, which can be used to optimize the flight track for efficient mapping of ozone and aerosol plumes. Data are stored for more detailed post-flight processing. A description of the lidar components is given in the following sections, and a schematic diagram of the lidar system is shown in Figure 2.

*a. Laser and transmitter*

The lidar transmitter is based on a compact solid-state laser system originally developed by Science and Engineering Services (SESI) for NASA Langley under a Small Business Innovative Research (SBIR) program (Fromzel and Prasad 2003; Prasad et al. 2006; Fromzel et al. 2007). The laser system uses a commercial laser (Coherent Evolution TEM00) to pump the custom laser section developed by SESI. The TEM00 is a diode-pumped, neodymium-doped yttrium lithium fluoride (Nd:YLF) laser operating at a fundamental wavelength of 1053 nm. Intracavity frequency doubling in a lithium triborate (LBO) crystal generates a 527 nm output beam that is directed into the SESI laser where it is again frequency doubled in a cesium lithium borate (CLBO) crystal. The resulting 263 nm beam then pumps a tunable cerium-doped lithium calcium aluminum fluoride (Ce:LiCAF) laser. The final laser output can be tuned from approximately 283 nm to 310 nm with a bandwidth of 0.2 nm, pulse-to-pulse wavelength stability of <0.1 nm, pulse repetition rate of 1000 Hz, and a pulse width of 100 ns. The laser is controlled via computer interface, and can be tuned on a pulse-to-pulse basis. This is

accomplished by controlling the timing of the laser trigger relative to the position of an oscillating galvo-mounted end-mirror in the Ce:LiCAF cavity. This oscillating mirror in conjunction with a tuning prism in the Ce:LiCAF cavity enable the rapid tuning of the laser. For TOPAZ, the laser is configured for 3-wavelength operation with each of the wavelengths generated sequentially in the order:  $\lambda_1, \lambda_2, \lambda_3, \dots$ . Thus, each of the wavelengths is separated in time by 1 ms and a complete set of wavelengths is generated at a repetition rate of 333 Hz. The wavelengths are monitored by a fiber-coupled spectrograph that samples a portion of the Ce:LiCAF output beam.

The laser has peak output energy at  $\sim 290$  nm which then drops to half-power at  $\pm 5$  nm from the peak, however by varying the relative timing of the pulses to allow more pump buildup time, the longer wavelength outputs (needed as mentioned in the analysis section below) can be strengthened at the expense of the near-peak wavelength outputs. The laser is typically operated with an average output pulse energy of  $\sim 0.1$  mJ pulse<sup>-1</sup> (with the longer wavelength pulses having 30 to 85% of the energy that the near-peak wavelength pulses have, depending on the wavelengths and the timing parameters set) which is less than the maximum rated output of 0.2-0.8 mJ pulse<sup>-1</sup> (depending on wavelength) in order to reduce optical damage to the components within the laser. Table 1 includes a summary of the laser and lidar specifications. Several components have been found to develop surface optical damage from the 263 nm pump light. These include a pair of calcium fluoride prisms used to separate the 263 nm light from the residual 527 nm light after the fourth harmonic generation, the lenses and mirrors in the pump beam path, and the Ce:LiCAF crystal itself. Even with the reduced operating

power, it is still necessary to re-position (or replace) the optics and crystal periodically (after ~30 hours of laser operation for the prisms, longer for other components) to move the damaged surfaces out of the beam path. The laser was designed with the capability to translate the Ce:LiCAF crystal due to damage issues, but additional modifications have been made to the laser including the ability to translate the prisms mentioned above when they become damaged.

The ~1 mm diameter laser beam is sent through a 5x beam expander (BE1, in Figure 2) which is adjusted to set the beam divergence to ~0.5 mrad (full angle), making the transmitted beam eye-safe at ranges greater than 200 m. The expanded beam is reflected from a transmitter mirror (M3, in Figure 2) located on-axis of, and directly behind the secondary mirror of the receiver telescope. The transmitter mirror can be remotely adjusted in flight using piezoelectric-driven adjustment screws to optimize the overlap between the laser beam and the receiver field of view. This optimization is accomplished by looking at a computer display of the graph of  $\ln(S * r^2)$  versus  $r$ , where  $S$  is the signal at range  $r$  from the lidar, (resulting in an approximately linear graph for a uniform atmosphere) and making laser pointing adjustments until both the near and far field signals are maximized.

#### *b. Receiver and detectors*

The lidar receiver uses an f/2 0.5 m diameter, lightweight (honeycombed) mirror in a Newtonian telescope to collect the backscattered laser light. Since the return signals decay rapidly ( $\sim r^{-2}$ ) at close range, two techniques are implemented to accommodate the

large dynamic range. First, a beamsplitter (BS2, in Figure 2) divides the collected light into near-field (NF) and far-field (FF) channels. The first aperture (A1, in Figure 2) sets the field of view (FOV) for the near-field channel to 3.0 mrad to allow full overlap of the transmitted laser light with the receiver FOV  $\sim 300$  m from the lidar, while a second aperture (A2, in Figure 2) sets the FOV for the far-field channel at 1.5 mrad resulting in complete overlap at  $\sim 800$  m. To compensate for the peak signal differences, the beamsplitter directs more (90%) of the received light to the far-field channel. In addition to these "passive" dynamic range compression techniques, a computer-controlled variable gain amplifier (VGA) after each detector can change the gain settings between each pulse (and thus wavelength). This allows dynamic adjustment for the differences in signal level due to variations in the laser pulse energy as a function of wavelength as well as the increased atmospheric attenuation of the shorter wavelengths in high ozone conditions. The variable gain amplifier settings span 0 to 31 dB gain and the typical variations of the signals from each channel/wavelength combination require settings ranging from 24 to 31 dB. The implementation of the near- and far-field channels along with the programmable amplifiers allows for better matching of the very different return signal amplitudes to the full-scale digitizer range.

Both detector channels use Hamamatsu R2076 photomultiplier tubes (PMTs) that have been tested and selected for very linear response when operated in voltage divider bases that have been optimized for gated operation. The PMTs are operated in an analog (current source) mode and are gated to reduce saturation and signal-induced bias (SIB) effects and thus providing enhanced pulsed response linearity (Lee et al. 1990; Bristow et

al. 1995; Zhao 1999; Bristow 2002; Machol et al. 2009). The optical paths to both detectors have short-pass filters (Barr Associates,  $\lambda_{\text{pass}} \leq 301$  nm) that reduce the solar background light within the PMT spectral sensitivity range by a factor of  $10^6$  while transmitting  $>65\%$  of the backscattered UV laser light.

*c. Computer controls and data acquisition*

The control and data acquisition tasks are distributed among three computers in the system. All three computers use solid state drives for operation in the unpressurized Twin Otter since traditional hard drives are unreliable at altitudes above about 3 km. The first computer handles the direct control of the lasers and was provided as part of the SESI laser system. This computer controls the pump laser current, the wavelength scanning/tuning, pulse timing, etc. along with providing outputs to monitor the laser operating status and wavelengths as well as generating timing pulses to synchronize the data acquisition system to the laser output.

The second computer provides the principal data acquisition components. This computer includes a custom field programmable gate array (FPGA) that is configured with two 14-bit digitizers that operate at a 100 MHz sample rate. This corresponds to a dwell time of 10 ns or an atmospheric range resolution of 1.5 m. This resolution is higher than that provided by the 100 ns laser pulse, but the signals are averaged as described below. The signals are digitized over a range of 0 to  $\sim 11.5$  km so that the farthest range gates (corresponding to ranges beyond ground level in nadir-looking airborne operation) may be used to determine the background signal level due to scattered light, amplifier offset,

etc. The FPGA also accumulates the signals in range (to range gates of 6 m and resulting in 16-bit values) and accumulates the signals in time (to a 5 Hz data rate). This accumulation helps reduce the statistical noise in the signals and decreases the rate at which data are written to the drives. The accumulation steps include a check whether signals are between lower and upper threshold levels that can be set by the user. The portions of the signals that are found to be out-of-range (e.g. due to strong backscatter signals from clouds) are not accumulated into the 5 Hz data. The number of samples that were accumulated at each 6-m range gate is stored together with the 5 Hz data so that the correct signal averages can be calculated prior to the aerosol and ozone calculations as described in the analysis section below. The FPGA also keeps track of the wavelengths to check for missed laser pulses or missed triggers to the data system, and controls the settings of the VGAs mentioned in the receiver description section above. This computer also provides an interface to a low-speed digitizer used to sample in situ measurements of temperature, pressure, and ozone concentration at flight level as well as surface (land/water) skin temperature measured with a nadir-pointing infrared pyrometer (Heitronics KT15.85D). (These extra measurements provide contextual information that can be used in the later application and analysis of the ozone and aerosol data provided by the lidar.) All of the data is then transferred to the third computer via a network connection.

The third computer is responsible for saving the raw data to the disk drives and performing a preliminary analysis of the ozone and aerosol profiles (as described below)

for real time feedback to the lidar operators on board. This computer also includes a GPS receiver that provides time and location stamps for the lidar data records.

### **3. Airborne operation**

Operation of a lidar or other sensitive optical instrument on an unpressurized airborne platform poses many challenges beyond those found in a laboratory environment. These include significant limitations on the instrument size and weight along with the need for operation in a harsh environment that includes high noise and vibration along with wide variations in ambient temperature and pressure. In addition to the technical requirements for the lidar operation, safety and structural requirements need to be met for airworthiness certification from the appropriate agencies.

The TOPAZ lidar system is designed to fly aboard relatively small aircraft platforms such as the DeHavilland DHC-6 Series 300 Twin Otters operated by the NOAA Aircraft Operations Center (AOC). These aircraft typically fly at altitudes below ~5 km MSL at a mean survey speed of ~60 m s<sup>-1</sup>. The aircraft is crewed with two pilots, and there are typically two or three lidar operators on board. The entire TOPAZ system has a gross weight of ~400 kg or ~46% of the useful Twin Otter payload of 865 kg. (Individual component weights and sizes are given in Table 1.) This allows enough fuel for typical research flights of up to 6 hours duration depending on the individual aircraft fuel tank configuration and what additional equipment is installed. The lidar and its components are secured to the seat mounting tracks in the aircraft cabin (Figure 1). The main lidar structure containing the lasers and optics is modeled after the older NOAA airborne

ozone lidar (Alvarez et al. 1998) and is attached to the tracks by shock-absorbing mounts to reduce vibrations transmitted from the airframe to the laser. The closed-loop chiller for the laser is mounted separately on the tracks, and the computers and control electronics are housed in 19-inch equipment racks certified for aircraft use. The electrical power required to operate the entire system is approximately 3 kW.

Since the Twin Otter is unpressurized and the lidar port does not have a window (a large and expensive fused silica window would be required for transmission in the UV range), large variations in the temperature and pressure surrounding the lidar are experienced during flight. The initial test flights of the lidar revealed that these environmental changes caused significant variations in the laser alignment and the temperature control of the nonlinear crystals, resulting in reduced laser power and optical damage to several of the internal laser components. To reduce these effects, a baffle system (consisting of plywood and flexible tape that seals the gap between the edge of the telescope tube and the edge of the hole in the aircraft floor) was added to reduce the amount of cold outside air that blows onto the laser, and a temperature control system with thermal insulation was added to the laser housing to better stabilize the laser temperature. Additionally, the laser housings were sealed so that a pressure control system can be used to maintain near-ground-level pressure within the laser cavity.

#### **4. Signal Processing**

After the digitized and accumulated lidar signals from the FPGA are stored on the disk drives, these raw TOPAZ data undergo several processing steps prior to the DIAL analysis.

*a. Averaging and basic corrections*

The 5 Hz data records for each wavelength and the near and far channels from the FPGA are first averaged to 1 s time resolution (while maintaining the 6 m data resolution). (Note that the 100 ns pulse length dictates that independent data points are  $\geq 15$  m apart, but the data is kept at 6 m resolution since it is still useful in identifying thin layers or edges of layers even though some smearing of these features will occur.) The average signal over 100 range gates at a range of  $\sim 10$  km is used to determine the signal offset for each of the six return signals. For nadir-viewing airborne operation, this offset reference range is several kilometers beyond the ground return spike. Next, the electromagnetic interference (EMI) noise associated with laser firing and other synchronous processes is subtracted from each of the six signals. Since the laser system has no flashlamps, the EMI is relatively small and reproducible and generally does not change much over the course of a flight. The EMI noise is determined about every 30 min by blocking both the outgoing laser beam and the main receiver aperture (A1, in Figure 2) for about 1 min. The averaged EMI file nearest in time is subtracted from each 1-s signal trace.

The offset- and EMI-corrected near and far channel data are concatenated to form 'blended' signals for each wavelength. The blending region is typically set at 1100 to 1200 m range or about 300 m beyond the point where the laser beam and the far channel

field of view completely overlap. The far channel data are then scaled to match the near channel data in the blending region. Additionally, since there is no information about the pointing angle of the laser beam during aircraft turns, these periods are identified from the GPS data and the lidar data discarded. Aircraft attitude information is not recorded except for a simple measurement of the typical aircraft pitch during flight which is then used to account for the slightly off-nadir pointing of the laser beam during straight flight legs.

Cloud tops and the ground location are identified using the blended data at the longest wavelength, which is least attenuated by ozone. A spike in the signal qualifies as a hard target return from a cloud or the ground when the derivative (with respect to range) of the range-squared corrected signal (normalized to the signal at 300 m range) exceeds an empirically determined threshold value. The data for all three wavelengths at and beyond three range gates (18 m) above cloud top or the ground are discarded.

*b. Signal induced bias and amplifier overshoot correction*

Since the offset- and EMI-corrected signals should be zero beyond a hard target return, any deviations in the baseline must be due to SIB in the PMTs or nonlinearities in the amplifier response. Signal-induced bias or afterpulsing is a well known problem in lidar systems that appears as one or more exponentially decaying tails in the anode current following exposure of a PMT to a short light pulse (Lee et al. 1990). However, laboratory and field measurements show that amplifier overshoot is generally larger than SIB in the TOPAZ detection system as can be seen from the typical signal trace showing

the ground return spike in Figure 3. The maximum negative bias in the baseline beyond a hard target spike is generally only about one or two digitizer counts or  $\sim 10^{-4}$  of the full scale signal, except when the hard target is close to the aircraft as during takeoff or landing, or when clouds are encountered near the aircraft. However, if improperly corrected, even this small overshoot can cause significant biases in the retrieved ozone concentrations at maximum range in the lowest several hundred meters above ground where the return signals are weak due to strong attenuation by ozone and aerosols (Figure 3). The companion paper by Langford et al. (2011) discusses this potential source of error in more detail.

Since some SIB is convolved with the overshoot in the amplified PMT signals, both biases are corrected by empirically fitting an exponential function to the negative signal just beyond the ground spike (Figure 3). This function is then extrapolated to the first range gate and subtracted from the lidar signal. The best results are obtained using a function of the form  $f(r) = a_1 \exp(-b \cdot r) + a_2 \cdot r + a_3$ , where  $r$  is the range gate number and  $a_1$ ,  $a_2$ , and  $a_3$  are the fit parameters. The function  $f(r)$  is fitted to the ‘tail’ of the blended signal for each wavelength from 360 m beyond the hard target return to 10000 m range. The exponent  $b$  is fixed, so that when extrapolated to the first range gate the fit function does not vary too greatly from one 1-s profile to the next. A mean value of  $b = 0.007$  was determined by a simple exponential fit of the form  $a \cdot \exp(-b \cdot r)$ . To reduce noise in the data for the fitting process, the 1-s data are averaged by a 60 s gliding filter ( $\pm 30$  s), except at the beginning or end of the data set.

Prior to the ozone and aerosol backscatter retrieval, the blended 1-s lidar signal data, now corrected for offset, EMI, and baseline deviations, and screened for aircraft turns and hard target returns due to the ground and clouds, are averaged in time over 10 s. This results in a horizontal resolution of 600 m at the typical Twin Otter survey speed of  $\sim 60 \text{ m s}^{-1}$ .

## **5. DIAL Analysis**

Ozone profiles are computed from the processed TOPAZ lidar data using the DIAL technique (Schotland 1974; Browell et al. 1985). This technique determines range-resolved concentrations through time-dependent differences in the backscattered light at two wavelengths absorbed to different degrees by the molecule of interest, i.e. ozone. (The two wavelengths are generally referred to as the on-line and off-line wavelengths for the more absorbed and less absorbed wavelengths respectively.) The Hartley absorption band between  $\sim 260$  and 300 nm in the near UV is the spectral region of choice for lidar measurements of tropospheric ozone, and the vast majority of past and current tropospheric ozone lidar systems use UV laser transmitters operating in this range (e.g. Grant and Hake 1975; Pelon and Megie 1982; Browell et al. 1983; Uthe et al. 1992; Proffitt and Langford 1997; Richter et al. 1997; Weidauer 1997; Alvarez et al. 1998; Ancellet and Ravetta 1998; Fix et al. 2002, Meister et al. 2003; Machol et al. 2009). Longer wavelengths are typically used for stratospheric measurements. The TOPAZ lidar is unique, however, in that it employs a tunable ultraviolet laser that transmits three wavelengths, which allows the instrument to be optimized for differing atmospheric conditions and to use alternate analysis techniques. This optimization includes the ability

to select wavelengths that have appropriate amounts of absorption for the concentration of ozone present in the atmosphere, to minimize the interference by other trace gas constituents such as sulfur dioxide (SO<sub>2</sub>), and to use advanced, multi-wavelength analysis techniques.

The full tuning range of the TOPAZ laser extends from about 283 to 310 nm, which covers much of the Hartley absorption band (Figure 4). However, laser pulse energies below ~286 nm and above 300 nm are very low (when operated at the reduced power setting described in Section 2) and not suitable for DIAL measurements. In addition, the cutoff filters in the receiver section block light at wavelengths greater than 301 nm. Therefore, the three TOPAZ wavelengths are typically set in the ranges:  $286 \leq \lambda_1 \leq 289$  nm,  $292 \leq \lambda_2 \leq 296$  nm, and  $296 \leq \lambda_3 \leq 300$  nm. Wavelengths at the lower end of the respective ranges, corresponding to stronger attenuation of the laser light by ozone, are chosen when low to moderate atmospheric ozone levels are expected. Longer wavelengths that are less attenuated by ozone are used under high ambient ozone conditions. Measurements with optimized wavelength pairs have yielded ozone profiles with good precision under a variety of atmospheric conditions with ozone levels ranging from 20 ppbv in clean marine air to more than 200 ppbv in polluted urban air masses.

Although any combination of the three TOPAZ wavelengths can be used to retrieve ozone profiles with the standard, 2-wavelength DIAL technique, most measurements are made using the  $\lambda_1$ - $\lambda_3$  wavelength pair, because it yields data with good signal-to-noise ratios (SNRs) over a wide range of atmospheric conditions. To minimize interference by

SO<sub>2</sub> we choose the on- and off-line wavelengths in such a way that the differential SO<sub>2</sub> absorption cross-section is very small (Figure 4). As a result, the bias in the ozone retrieval due to SO<sub>2</sub> interference is less than about 1 ppbv even when high concentrations of SO<sub>2</sub> are present. TOPAZ can also be configured to measure SO<sub>2</sub> simultaneously with ozone. For example, when tuned to 288.8, 299.3, and 300.0 nm, the  $\lambda_1$ - $\lambda_3$  wavelength pair can be used as usual for the ozone retrieval, while  $\lambda_2$  and  $\lambda_3$  serve as off- and on-line channels for the DIAL SO<sub>2</sub> retrieval (Figure 4). The third wavelength ( $\lambda_3$ ) is centered on the peak of the strongest SO<sub>2</sub> absorption line in the near UV spectral region, while  $\lambda_2$  is tuned to a region of low SO<sub>2</sub> absorption adjacent to the absorption line. The first wavelength is tuned to the peak of another SO<sub>2</sub> absorption line, resulting in a small differential SO<sub>2</sub> absorption cross-section for the  $\lambda_1$ - $\lambda_3$  pair and thus minimizing the SO<sub>2</sub> interference on the ozone retrieval. The ozone measurements can be used to correct for the interference of ozone on the SO<sub>2</sub> retrieval. Cao et al. (2006) describe a similar approach to measure atmospheric ozone and SO<sub>2</sub> concentrations simultaneously, however they used a dye laser system to generate tunable wavelengths in the UV spectral region. Future tests are planned to determine whether TOPAZ is suitable for atmospheric SO<sub>2</sub> measurements and what precision and accuracy can be expected. In particular, we will assess whether the wavelength stability (better than 0.1 nm) and laser line width (0.2 nm) of TOPAZ are sufficient for SO<sub>2</sub> retrieval, which makes use of rather narrow absorption features (FWHM  $\approx$  1 nm) compared to the broad Hartley absorption band used in the ozone DIAL measurements.

Ozone retrievals with the standard 2-wavelength DIAL technique may be biased due to differences in aerosol extinction and backscatter between the two DIAL wavelengths (Browell et al., 1985). These differential aerosol effects can be corrected by using aerosol information from the longer off-line DIAL wavelength, but uncertainties remain. As an alternative to the standard DIAL technique, ozone profiles can also be calculated using the 3-wavelength dual-DIAL technique (Kovalev and Bristow 1996; Wang et al. 1997). The tunability of TOPAZ allows us to choose the appropriate spacing between the three wavelengths to optimize the dual-DIAL retrieval. As Kovalev and Bristow (1996) and Wang et al. (1997) have shown, this method significantly reduces the uncertainties in the ozone retrieval due to aerosol effects. In fact, this technique does not require any information about aerosol properties in order to retrieve ozone profiles. However, this convenience comes at the expense of significantly increased noise in the ozone data compared to the 2-wavelength DIAL technique. Therefore, we generally use the standard DIAL technique, except under conditions when a satisfactory estimate of the aerosol properties required for the differential aerosol correction cannot be obtained. Another 3-wavelength technique to retrieve ozone profiles has been described by Eisele and Trickl (2005). In addition to ozone concentration and aerosol backscatter, their approach also yields estimates of extinction-to-backscatter ratio and wavelength dependences of aerosol backscatter and extinction. This analysis technique appears to be quite sensitive to statistical noise in the data and generally requires longer averaging times than what is feasible for the airborne TOPAZ lidar. Therefore, we did not consider using this technique for the TOPAZ lidar data retrieval.

*a. Ozone retrieval and aerosol correction*

As mentioned above, ozone retrieval using the  $\lambda_1$ - $\lambda_3$  wavelength pair requires correction of potential biases due to differences in aerosol extinction and backscatter between the two DIAL wavelengths. As described by Browell et al. (1985), these biases can be particularly large in regions of strong aerosol gradients, which typically occur near clouds or at the top of the planetary boundary layer. These differential aerosol effects are explicitly corrected using aerosol backscatter and extinction profiles derived from the  $\lambda_3$  data following the approach of Fernald (1984) and assuming backscatter and extinction wavelength dependences. However, since ozone extinction is still significant at wavelengths between 296 and 300 nm and is comparable to the extinction due to aerosol and Rayleigh scattering, the  $\lambda_3$  aerosol data also have to be corrected for ozone extinction. Immler (2003) suggested an algorithm, the so-called Klett-DIAL method, which allows computation of ozone and aerosol backscatter profiles simultaneously. This technique was demonstrated using simulated ozone DIAL data for two closely spaced DIAL wavelengths with a separation of 3.5 nm. However, it is unclear how well this technique would work with measured DIAL data that are subject to noise and what the implications of the larger TOPAZ wavelength spacings ( $\sim 10$  nm) would be. For these reasons, we chose a scheme that computes ozone and aerosol backscatter profiles iteratively until the measured ozone concentrations converge. For the first step in our iteration, we compute preliminary ozone profiles, generally using the  $\lambda_1$ - $\lambda_3$  wavelength pair, without any differential aerosol backscatter and extinction correction. For the DIAL calculation, only data beyond 400 m range (when the telescope field of view and the lidar beam are in full overlap) are used and the lidar signals are averaged range-wise over 90 m. The derivative

in the DIAL equation is computed as the slope of the least squares linear fit over five adjacent 90-m gates and the resulting ozone value is assigned to the middle gate. This process is repeated in a gliding fashion over the entire measurement range. At the edges of the measurement range, three and two adjacent 90-m gates are used for the ozone calculation at the next-to-last and last gates, respectively. The reported ozone range resolution is 90 m, and layers of this thickness are still visible in the data, however, completely independent data points are spaced 450 m apart. The preliminary ozone profiles are used to correct the lidar data at  $\lambda_3$  for ozone extinction, and these corrected data are utilized to compute aerosol backscatter and extinction profiles. The aerosol data are retrieved at an 18 m resolution. To compute aerosol backscatter and extinction profiles from single wavelength lidar data, an aerosol backscatter reference value at a given range and the extinction-to-backscatter ratio have to be prescribed (e.g. Fernald 1984). For the aerosol backscatter reference range, it is advisable to use a region at the far end of the measurement range (close to the surface for the nadir-looking TOPAZ lidar) because otherwise the aerosol backscatter retrieval may become computationally unstable. Therefore, we typically choose a region within the boundary layer a few hundred meters above ground level. The aerosol backscatter reference value and the extinction-to-backscatter ratio (which is usually assumed constant with altitude) are estimated based upon collocated measurements of aerosol properties (if available) or literature values for the type aerosol (urban, continental, maritime, dust) that is assumed to be prevailing during the measurement. The aerosol backscatter and extinction wavelength dependences, which are needed to correct differential aerosol effects in the ozone calculation, are assumed to follow a power law. In most cases, we use a power law

exponent of 0 (no wavelength dependence) for aerosol backscatter and an exponent of -0.5 for aerosol extinction. These values seem to be a good compromise for a wide range of aerosol types (Völger et al. 1996).

In the second iteration step, ozone profiles are computed with aerosol correction using the aerosol backscatter and extinction profiles from the first step. These ozone profiles are then used to provide a more accurate ozone extinction correction of the signal data at  $\lambda_3$ , which in turn results in a more accurate aerosol profile retrieval. This iteration procedure is repeated until the ozone profiles produced in successive iteration steps converge. Convergence is reached when the absolute difference between successive ozone profiles is less than  $2.5 \cdot 10^{15} \text{ m}^{-3}$  (corresponding to about 0.1 ppbv) at all range gates. The DIAL retrieval yields ozone profiles in units of number density. To convert these data to ozone mixing ratio, we use temperature and pressure fields initially from standard atmosphere profiles, and once available ( $\sim 1$  month delay), from the National Centers for Environmental Prediction/Climate Data Assimilation System (NCEP/CDAS) re-analysis data (Kalnay et al. 1996) at a spatial resolution of 1 x 1 degrees. Temperature and pressure information is also required to compute Rayleigh backscatter profiles (which are needed for the aerosol retrieval) and to account for temperature dependence of the ozone absorption cross-sections. Over the TOPAZ tuning range used for the ozone DIAL retrieval, ozone absorption cross sections vary by less than 0.2 % per degree K. Temperature and geopotential height data at pressure levels of 1000, 925, 850, 700, and 600 hPa are averaged spatially over the area covered by a given flight (or several segments of a flight, if the covered area is significantly larger than 1 x 1 degrees) and

then interpolated in altitude to yield average temperature and pressure profiles for a given flight.

During research flights, the TOPAZ data are analyzed in near real time using an abbreviated version of the analysis procedure described above for the real time display. No baseline correction is made and data collected during aircraft turns or beyond cloud or ground hard target returns are included. Temperature and pressure information is taken from standard atmosphere profiles. The preliminary ozone and aerosol backscatter profiles are displayed as a continuously updated curtain plot to allow the TOPAZ operators to make adjustments to the flight track or altitude in order to optimize the data collection.

*b. Systematic errors*

The retrieved ozone concentrations are subject to several other potential sources of error in addition to those discussed above. In particular, the retrieved concentrations are directly proportional to the reciprocal of the ozone differential absorption cross-sections. To select the most appropriate ozone absorption cross-section data for the DIAL retrieval, we conducted a review of several data sets including those of Bass and Paur (1985), Molina and Molina (1986), Malicet et al. (1995), Burrows et al. (1999), and Bogumil et al. (2003). These data sets are available at the database of the Max Planck Institute for Chemistry in Mainz, Germany (<http://www.atmosphere.mpg.de/enid/2295>). The ozone cross-section measurements by these five authors are reported at different wavelength resolutions and for various sets of temperatures ranging generally from 203 to 298 K.

We excluded the Molina and Molina (1986) data set because of its rather coarse wavelength resolution of 0.5 nm, compared to 0.01 to about 0.11 nm for the other data sets. The remaining four data sets were interpolated to 0.01 nm, and at each wavelength step, a quadratic fit of the absorption cross-section as a function of temperature was performed. Over the TOPAZ wavelength range of 286 to 300 nm, the interpolated absorption cross-section data sets have maximum deviations from the mean (four data set average) of about  $\pm 1.8\%$  for temperatures ranging from 283 to 313 K, which covers the ambient temperatures encountered during the TOPAZ field campaigns. Absolute mean differences (averaged over the TOPAZ wavelength range) from the mean are less than 1%. From the four absorption cross-section data sets that we compared, we selected the Burrows (1999) data set following a recommendation of the 2006 Jet Propulsion Laboratory (JPL) report on Chemical Kinetics and Photochemical Data for Use in Atmospheric Studies (Sander 2006). Based on our comparison study, we estimate the accuracy of the Burrows data to be better than 2%. This uncertainty in the absorption cross-section data translates into a bias of the same magnitude in the ozone retrieval.

The accuracy of the ozone retrieval is also affected by a number of other factors. Biases in the ozone retrieval due to uncertainties in the atmospheric temperature and pressure profiles taken from the NCEP CDAS reanalysis data are estimated to be about 2% and 0.5%, respectively. The TOPAZ wavelengths tend to drift very slightly over the course of a research flight. As a result, the wavelength differential  $\Delta\lambda = \lambda_1 - \lambda_3$  has an uncertainty of less than 0.1 nm, which translates into an error in the ozone retrieval of  $\leq 1\%$ . To estimate the effect of uncertainties in the baseline correction on the ozone

retrieval, we vary the SIB/overshoot correction parameters within reasonable bounds, perform the full DIAL calculation with these modified parameters, and use the differences in the resulting ozone profiles as an indicator for the associated uncertainties. For the SIB/overshoot correction we vary the fixed exponent,  $b$ , in the fit function ( $f(r) = a_1 \cdot \exp(-b \cdot r) + a_2 \cdot r + a_3$ , as described earlier) from 0.0065 to 0.0075 around the mean value of 0.007. Residual errors in the ozone calculation due to inaccuracies in the SIB/overshoot correction are typically in the 2-3% range, but under low signal-to-noise ratio conditions (i.e. at ranges  $>2.5$  km with high ozone concentrations), the errors can be as large as 15% as is shown in the companion paper by Langford et al. (2011). Under low SNR conditions, applying the correction can result in a relatively large change in signal levels (Figure 3b), and thus any uncertainties in the correction may result in larger residual biases in the signal levels and, in turn, the ozone calculations. To estimate the magnitude of the residual errors of the aerosol correction on the ozone retrieval, we varied the assumed aerosol backscatter wavelength dependence between  $\lambda^{-1}$  and  $\lambda^1$ . The wavelength dependence of aerosol extinction is held fixed at  $\lambda^{-0.5}$ , since models indicate that for typical aerosol mixtures the power law exponent is close to -0.5 (Völger et al. 1996). While variations in the extinction-to-backscatter ratio and aerosol backscatter reference value can lead to significant changes in the aerosol backscatter and extinction profiles, the impact on the ozone retrieval is generally small. Errors in the correction of differential aerosol effects depend on the actual aerosol spatial distribution encountered during a flight. They are generally most pronounced in regions of strong vertical aerosol gradients and can be as large as a few ppbv.

### *c. Statistical uncertainties*

The statistical uncertainty or precision of the TOPAZ ozone measurements is computed by using the autocovariance method (Lenschow et al. 2000) on the ozone time series data at each range gate. Prior to applying the autocovariance method, the data at each range gate are linearly detrended. We calculate the ozone root mean square (RMS) error for each time step and at each range gate by applying the autocovariance method to a 10 min window of data for a given range gate that is moved in a gliding fashion across the time series at each range. Ozone RMS errors increase with range away from the lidar due to the increasing extinction of the lidar signal and thus decreasing signal-to-noise ratio. The precision of the ozone retrieval also usually varies with time over the course of a flight depending on the ambient ozone and aerosol levels and changes in the laser output power. For ozone retrievals at the standard vertical resolution of 90 m and time resolution of 10 s, the overall error is dominated by statistical uncertainties. The  $1\sigma$  statistical errors typically vary from 2-5 ppbv (5-8%) at ranges close to the lidar and can range from 5-35 ppbv (12-30%) at ranges of 2.5 km and beyond, with the largest uncertainties occurring under low SNR conditions at large ranges with high ozone concentrations. The precision of the ozone measurements can be improved substantially by averaging over longer time intervals or larger range bins (Langford et al. 2011).

## **6. Measurements and Validation**

The TOPAZ lidar has been deployed on one of the NOAA Twin Otter aircraft during several field experiments since 2006, including the second Texas Air Quality Study (TexAQS 2006) (Parrish et al. 2009; Langford et al. 2010b; Senff et al. 2010; Banta et al.

2011), the 2008 Front Range Air Quality Study (Senff et al. 2009), the 2009 Pre-CalNex study (Langford et al. 2010a), and the CalNex 2010 experiment. During these studies, TOPAZ was successfully used to investigate the three-dimensional distribution of urban ozone and aerosol plumes, to estimate the horizontal flux of ozone from urban areas, to characterize the transport of ozone in and near complex terrain, and to determine the spatial distribution of the planetary boundary layer height. Figure 5 shows an example of the data collected with TOPAZ during the TexAQS 2006 experiment. In this case, we used TOPAZ to characterize the structure of the urban ozone plume and the horizontal ozone flux downwind of Houston, TX. More detailed information about this case can be found in Senff et al. (2010).

As an illustration of the performance of TOPAZ during TexAQS 2006, we have compared TOPAZ profiles with those measured by electrochemical cell (ECC) ozonesondes launched from the University of Houston campus as part of the IONS/INTEX sampling program (Thompson et al. 2008; Rappenglück et al. 2008; Morris et al. 2010). One of these launches occurred at 1829 UT on the afternoon of 31 August as the Twin Otter flew near the launch site. The area surrounding the launch site is shown in detail in Figure 6, along with the flight track of the northbound Twin Otter. The black squares represent the center locations of the individual 10-s TOPAZ profiles; the filled squares show the three profiles closest to the launch site (red circle). The dotted red line shows the ground track of the ozonesonde as it ascended from the surface to 4 km MSL. A plume of high ozone advected northwestward from the Houston Ship Channel by the Bay breeze passed to the south of the University during the afternoon (Langford et al.

2010b). This is seen more clearly in Figure 7, which shows a latitude-height curtain plot of the TOPAZ ozone profiles along the Twin Otter flight track from Figure 6. The black squares once again represent the locations of the TOPAZ profiles with the filled black squares and the dashed box indicating the profiles nearest the ozonesonde. The dotted black lines show the flight path of the ozonesonde launched at 1829 UT as the Twin Otter flew past. The profile is color-coded to show the measured concentration. The sea breeze front was located near the University of Houston at the time of the launch (Banta et al. 2005) and the balloon rose almost vertically to about 1500 m MSL, where it was blown southward over the ozone plume by strong northerly winds aloft (Figure 6). Figure 7 shows the value of the additional context provided by the lidar technique in areas with strong vertical and horizontal inhomogeneities in the ozone distribution. Also, note the increased scatter in the 10-s lidar measurements near the surface compared to the ozonesonde profile. This reflects the greater statistical uncertainty in these measurements.

The strong horizontal gradient in ozone at the edge of the plume limits the number of TOPAZ profiles that can be compared to the ozonesonde to three. Figure 8 plots the ozonesonde profile (red line), and the average (black line,  $\pm 1\sigma$ ) of the three TOPAZ profiles (gray lines) corresponding to the filled black squares and dashed boxes in Figures 6 and 7. The agreement between the two profiles is quite good except near the top of the plume where the 5-gate (450 m) smoothing of the DIAL profile degrades the vertical resolution. The small vertical displacement between the two profiles may reflect the

2 km horizontal averaging of the TOPAZ profile and the high spatial variability of the mixed layer height on 31 August (Langford et al. 2010b).

## **7. Summary and Conclusions**

The TOPAZ system represents a significant advancement in lidar for tropospheric ozone measurements. The incorporation of state-of-the-art UV laser technology makes the system uniquely flexible in terms of deployment and application. The tunable, 3-wavelength laser enables optimization of the lidar for differing atmospheric conditions, reduction of interference from other atmospheric constituents, and dual-DIAL operation. The high pulse rate and low pulse energy permit eyesafe, airborne operation while the smaller size, weight, and power requirements of the system have made deployment easier and less expensive. The performance of the TOPAZ lidar (Table 1) has been found to meet or exceed that of the prior NOAA airborne ozone lidar, and the data compare well with other instrumentation. With a resolution of 90 m (vertical) and 600 m (horizontal), the error in the ozone measurements is typically <5%, but can be as high as 15% under low SNR conditions at large ranges with high ozone concentrations. Similarly, the precision of the ozone measurements is typically  $\pm 2-5$  ppbv (5-8%) at ranges of 400-600 m and falls to  $\pm 5-35$  ppbv (12-30%) at ranges >2.5 km with the largest uncertainties occurring under low SNR conditions at large ranges with high ozone concentrations. The abilities of the TOPAZ lidar have been successfully demonstrated in the field, and the highly resolved measurements of ozone in the boundary layer and lower troposphere provided by the TOPAZ lidar have proven to be an exceptionally useful tool to study the 3-dimensional distribution of tropospheric ozone, to map out ozone plumes emanating

from urban areas or power plants, and to characterize ozone transport processes on local and regional scales.

### **Acknowledgments**

The authors would like to thank Brandi McCarty, Lisa Darby, and Joanne George for their help with TOPAZ data analysis and Gary Morris (Valparaiso University), Barry Lefer, Bernhard Rappenglueck, S. Boudreaux, B. Day, and L. Pedemonte (University of Houston) for providing the TexAQS 2006 ozonesonde data. We would also like to thank the crews of the NOAA Twin Otter and the NOAA Aircraft Operations Center (AOC).

The authors would also like to acknowledge support for TOPAZ from the NOAA Health of the Atmosphere program and the Texas Commission on Environmental Quality (TCEQ) (under grant 582-8-86246) and for support of the ozonesonde launches from TCEQ and the NASA Office of Earth Science.

### **Disclaimer of endorsement**

Reference to specific companies, trademarks, or proprietary products in this document is provided for information purposes only and does not constitute or imply endorsement by the authors, the National Oceanic and Atmospheric Administration, or the United States Government.

## References

Alvarez, R. J., II, C. J. Senff, R. M. Hardesty, D. D. Parrish, W. T. Luke, T. B. Watson, P. H. Daum, and N. Gillani, 1998: Comparisons of airborne lidar measurements of ozone with airborne in situ measurements during the 1995 Southern Oxidants Study. *J. Geophys. Res.*, **103**, 31,155-31,171.

Alvarez, R. J., II, W. A. Brewer, D. C. Law, J. L. Machol, R. D. Marchbanks, S. P. Sandberg, C. J. Senff, A. M. Weickmann, 2008: Development and Application of the TOPAZ Airborne Lidar System by the NOAA Earth System Research Laboratory, in *Proceedings of 24th International Laser Radar Conference*, Boulder, Colorado, USA, 23-27 June 2008, pp. 68-71.

Ancellet, G. and F. Ravetta, 1998: Compact airborne lidar for tropospheric ozone: description and field measurements, *Appl. Opt.*, **37**, 5509–5521.

Banta, R. M., C. J. Senff, J. Nielsen-Gammon, L. S. Darby, T. B. Ryerson, R. J. Alvarez, S. P. Sandberg, E. J. Williams, and M. Trainer, 2005: A bad air day in Houston, *Bull. Am. Met. Soc.*, **86**, 657-669.

Banta, R. M., C. J. Senff, R. J. Alvarez, A. O. Langford, D. D. Parrish, M. K. Trainer, L. S. Darby, R. M. Hardesty, B. Lambeth, J. A. Neuman, W. M. Angevine, J. Nielsen-Gammon, S. P. Sandberg, and A. B. White, 2011: Dependence of Daily Peak O<sub>3</sub>

Concentrations near Houston, Texas on Environmental Factors: Wind Speed, Temperature, and Boundary-Layer Depth, *Atmos. Environ.*, **45**, 166-173.

Bass, A.M., and R.J. Paur, 1985: The ultraviolet cross-sections of ozone: I. The measurements, in *Atmospheric Ozone: Proceedings of the Quadrennial Ozone Symposium*, Halkidiki, Greece, 3-7 September 1984, edited by C.S. Zerefos and A. Ghazi, pp. 606-610.

Bogumil, K., J. Orphal, T. Homann, S. Voigt, P. Spietz, O.C. Fleischmann, A. Vogel, M. Hartmann, H., Bovensmann, J. Frerick, and J.P. Burrows, 2003: Measurements of molecular absorption spectra with the SCIAMACHY pre-flight model: Instrument characterization and reference data for atmospheric remote sensing in the 230-2380 nm region, *J. Photochem. Photobiol. A.: Chem.* **157**, 167-184.

Bristow, M. P., D. H. Bundy, and A. G. Wright, 1995: Signal linearity, gain stability, and gating in photomultipliers: application to differential absorption lidars, *Appl. Opt.* **34**, 4437-4452.

Bristow, M. P., 2002: Suppression of afterpulsing in photomultipliers by gating the photocathode, *Appl. Opt.* **41**, 4975-4987.

Browell, E. V., A. F. Carter, S. T. Shipley, R. J. Allen, C. F. Butler, M. N. Mayo, J. H. Siviter, Jr., and W. M. Hall, 1983: NASA multipurpose airborne DIAL system and measurements of

ozone and aerosol profiles. *Appl. Opt.*, **22**, 522-534.

Browell, E. V., S. Ismail, and S. T. Shipley, 1985: Ultraviolet DIAL measurements of O<sub>3</sub> profiles in regions of spatially inhomogeneous aerosols, *Appl. Opt.*, **24**, 2827-2836.

Burrows, J.P., A. Richter, A. Dehn, B. Deters, S. Himmelman, S. Voigt, and J. Orphal, 1999: Atmospheric remote-sensing reference data from GOME: Part 2. Temperature-dependent absorption cross-sections of O<sub>3</sub> in the 231-794 nm range, *J. Quant. Spectrosc. Radiat. Transfer*, **61**, 509-517.

Cao, N, S. Li, T. Fukuchi, T. Fujii, R. L. Collins, Z. Wang, and Z. Chen, 2006: Measurement of tropospheric O<sub>3</sub>, SO<sub>2</sub> and aerosol from a volcanic emission event using new multi-wavelength differential-absorption LIDAR techniques, *Appl. Phys. B*, **85(1)**, 163-167.

Coutts, D. and A. J. S. McGonigle, 2004: Cerium-Doped Fluoride Lasers, *IEEE J. Quantum. Electron.*, **40(10)**, 1430-1440.

Eisele, H. and T. Trickl, 2005: Improvements of the aerosol algorithm in ozone lidar data processing by use of evolutionary strategies, *Appl. Opt.*, **44**, 2638-2651.

Elsayed, K. A., S. S. Chen, L. B. Petway, B. L. Meadows, W. D. Marsh, W. C. Edwards, J. C. Barnes, and R. J. DeYoung, 2002: High-energy, efficient, 30-Hz ultraviolet laser sources for airborne ozone-lidar systems. *Appl. Opt.*, **41**, 2734-2739.

Fernald, F. G., 1984: Analysis of atmospheric lidar observations: Some comments, *Appl. Opt.*, **23**, 652-653.

Fix, A., M. Wirth, A. Meister, G. Ehret, M. Pesch, and D. Weidauer, D., 2002: Tunable Ultraviolet Optical Parametric Oscillator for Differential Absorption Lidar Measurements of Tropospheric Ozone. *Applied Physics B*, **75**, 153-163. DOI: 10.1007/s00340-002-0964-y.

Fromzel V. A. and C. R. Prasad, 2003: A tunable, narrow linewidth, 1 kHz Ce:LiCAF laser with 46% efficiency, OSA Trends in Optics and Photonics, v.83, *Advanced Solid-State Photonics*, John J. Zayhowsky, ed. (OSA, Washington, DC), pp.203-209.

Fromzel, V. A., C. R. Prasad, K. Petrosyan, Y. Liaw, W. Shi, M. A. Yakshin, and R. DeYoung, 2007: Rapidly tunable, narrow linewidth, 1 W, 1 kHz Ce:LiCAF laser pumped by the fourth harmonic of a diode-pumped Nd:YLF laser for ozone DIAL measurements, *CLEO/QELS 2007*, 6-11 May 2007, Baltimore, USA, paper JWA84.

Grant, W. B., and R. D. Hake Jr., 1975: Calibrated remote measurements of SO<sub>2</sub> and O<sub>3</sub> using atmospheric backscatter, *J. Appl. Phys.*, **46**, 3019-3023

Immler, F., 2003: A new algorithm for simultaneous ozone and aerosol retrieval from tropospheric DIAL measurements, *Appl. Phys. B*, **76**, 593-596.

Kalnay, E., and coauthors, 1996: The NCEP/NCAR 40-Year Reanalysis Project, *Bull. Am. Meteorol. Soc.*, **77**, 437-471.

Kovalev, V. A. and M. P. Bristow, 1996: Compensational three-wavelength differential-absorption lidar technique for reducing the influence of differential scattering on ozone-concentration measurements, *Appl. Opt.*, **35**, 4790-4797.

Langford, A. O., C. J. Senff, R. J. Alvarez II, R. M. Banta, and R. M. Hardesty, 2010a: Long-range transport of ozone from the Los Angeles Basin: A case study, *Geophys. Res. Lett.*, **37**, L06807, doi:10.1029/2010GL042507.

Langford, A. O., S. C. Tucker, C. J. Senff, R. M. Banta, W. A. Brewer, R. J. Alvarez II, R. M. Hardesty, B. M. Lerner and E. J. Williams, 2010b: Convective venting and surface ozone in Houston during TexAQS 2006, *J. Geophys. Res.*, **115**, D16305, doi:10.1029/2009JD013301.

Langford, A. O., C. J. Senff, R. J. Alvarez II, R. M. Banta, R. M. Hardesty, D. D. Parrish, and T. B. Ryerson, 2011: Comparison between the TOPAZ airborne ozone lidar and in situ measurements during TexAQS 2006. *J. Atmos. Oceanic Technol.*, submitted.

Lee, H. S., G. K. Schwemmer, C. L. Korb, M. Dombrowski, and C. Prasad, 1990: Gated photomultiplier response characterization for DIAL measurements, *Appl. Opt.* **29**, 3303–3315.

Lenschow, D. H., V. G. Wulfmeyer, and C. J. Senff, 2000: Measuring second- through fourth-order moments in noisy data. *J. Atmos. and Oceanic Technol.*, **17**, 1330-1347.

Machol J. L., R. D. Marchbanks, C. J. Senff, B. J. McCarty, W. L. Eberhard, W. A. Brewer, R. A. Richter, R. J. Alvarez, D. C. Law, A. M. Weickmann, and S. P. Sandberg, 2009: Scanning tropospheric ozone and aerosol lidar with double-gated photomultipliers, *Appl. Opt.*, **48**, 512-524.

Malicet, J., D. Daumont, J. Charbonnier, C. Parisse, A. Chakir, and J. Brion, 1995: Ozone UV spectroscopy. II. Absorption cross-sections and temperature dependence, *J. Atmos. Chem.*, **21**, 263-273.

Meister, A., A. Fix, H. Flentje, M. Wirth, and G. Ehret, 2003: TropOLEX: A new tunable airborne lidar system for the measurement of tropospheric ozone, *6th International Symposium on Tropospheric Profiling*, Leipzig, 14-20 September 2003, pp. 233-235.

Molina, L.T. and M.J. Molina, 1986: Absolute absorption cross-sections of ozone in the 185- to 350-nm wavelength range, *J. Geophys. Res.* **91**, 14501-14508.

Morris, G. A., B. Ford, B. Rappenglück, A. M. Thompson, A. Mefferd, F. Ngan, and B. Lefer, 2010: An evaluation of the interaction of morning residual layer and afternoon mixed layer ozone in Houston using ozonesonde data. *Atmos. Environ.*, **44**, 4024-4034.

Parrish, D. D., et al. 2009: Overview of the Second Texas Air Quality Study (TexAQS II) and the Gulf of Mexico Atmospheric Composition and Climate Study (GoMACCS), *J. Geophys. Res.*, **114**, D00F13, doi:10.1029/2009JD011842.

Pelon, J. and G. Mégie, 1982: Ozone Monitoring in the Troposphere and Lower Stratosphere: Evaluation and Operation of a Ground Based Lidar Station, *J. Geophys. Res.*, **87**, 4947-4955.

Prasad C. R., V. A. Fromzel, W. Shi, C. S. Wilks, and R. DeYoung, 2006: A compact, rapidly tunable Ce:LiCAF DIAL transmitter for airborne ozone measurements, *23rd International Laser Radar Conference (ILRC)*, 24-28 July 2006, Nara, Japan, paper PD1-4.

Proffitt, M. H. and A. O. Langford, 1997: Ground-based differential absorption lidar system for day or night measurements of ozone throughout the free troposphere, *Appl. Opt.*, **36**, 2568-2585.

Rambaldi, P., Douard, M., and Wolf, J.-P., 1995: New UV Tunable Solid-State Lasers for Lidar Applications, *Appl. Phys. B*, **61**,117-120.

Rappenglück, B., R. Perna, S. Zhong, and G.A. Morris, 2008: An analysis of the vertical structure of the atmosphere and the upper-level meteorology and their impact on surface ozone levels in Houston, TX, *J. Geophys. Res.*, **113**, D17315, doi:10.1029/2007JD009745.

Richter, D. A., E. V. Browell, C. F. Butler, N. S. Higdon, 1997: Advanced airborne UV DIAL system for stratospheric and tropospheric ozone and aerosol measurements, in *Advances in Atmospheric Remote Sensing with Lidar*, ed. by A. Ansmann, R. Neuber, P. Rairoux, U. Wandinger (Springer, Berlin Heidelberg 1997), pp. 395-398

The Royal Society, 2008: Ground-level ozone in the 21st century: future trends, impacts and policy implications., 133 pp.

Sander, S. P., B. J. Finlayson-Pitts, R. R. Friedl, D. M. Golden, R. E. Huie, H. Keller-Rudek, C. E. Kolb, M. J. Kurylo, M. J. Molina, G. K. Moortgat, V. L. Orkin, A. R. Ravishankara and P. H. Wine, 2006: Chemical Kinetics and Photochemical Data for Use in Atmospheric Studies, Evaluation Number 15, JPL Publication 06-2, Jet Propulsion Laboratory, Pasadena.

Schotland, R. M., 1974: Errors in the Lidar Measurement of Atmospheric Gases by Differential Absorption, *J. Appl. Meteorol.*, **13**, 71-77.

Senff, C. J., R. J. Alvarez II, A. M. Weickmann, J. Brioude, W. A. Brewer, S. P. Sandberg, A. B. White, W. M. Angevine, S. A. McKeen, 2009: The Effect of Complex Terrain on Ozone Distribution and Transport in the Colorado Front Range Area, Proceedings of the *8th International Symposium on Tropospheric Profiling: Needs and Technologies*, ISBN 978-90-6960-233-2, Delft, The Netherlands, 19-23 October, 2009, S03-O05, 1-4, Editors, A. Apituley, H.W.J. Russchenberg, W.A.A. Monna.

Senff, C. J., R. J. Alvarez, II, R. M. Hardesty, R. M. Banta, and A. O. Langford, 2010: Airborne lidar measurements of ozone flux downwind of Houston and Dallas, *J. Geophys. Res.*, **115**, D20307, doi:10.1029/2009JD013689.

Thompson, A. M., J. E. Yorks, S. K. Miller, J. C. Witte, K. M. Dougherty, G. A. Morris, D. Baumgardner, L. Ladino, and B. Rappengluck, 2008: Tropospheric ozone sources and wave activity over Mexico City and Houston during MILAGRO/Intercontinental Transport Experiment (INTEX-B) Ozonesonde Network Study, 2006 (IONS-06). *Atmospheric Chemistry and Physics*, **8**, 5113-5125.

Uthe E., J. Livingston, and N. Nielsen, 1992: Airborne lidar mapping of ozone concentrations during the Lake Michigan ozone study, *J. Air Waste Manage. Assoc.* **42**, 1313–1318.

Vandaele, A.C., C. Hermans, and S. Fally, 2009: Fourier transform measurements of SO<sub>2</sub> absorption cross sections: II. Temperature dependence in the 29000-44000 cm<sup>-1</sup> (227-345 nm) region, *J. Quant. Spectrosc. Radiat. Transfer*, **110**, 2115-2126.

Völger, P., J. Bösenberg, and I. Schult, 1996: Scattering Properties of Selected Model Aerosols Calculated at UV-wavelengths: Implications for DIAL Measurements of Tropospheric Ozone, *Contr. Atmos. Phys.*, **69**, 177-187.

Wang, Z., H. Nakane, H. Hu, and J. Zhou, 1997: Three-wavelength dual differential absorption lidar method for stratospheric ozone measurements in the presence of volcanic aerosols, *Appl. Opt.*, **36**, 1245-1252,.

Weidauer D., P. Rairoux, M. Ulbricht, J.P. Wolf, L. Wöste, 1997: Ozone, VOC, NO<sub>2</sub>, and aerosol monitoring in urban and industrial areas using a mobile DIAL system, in *Advances in atmospheric remote sensing with lidar*, ed. by A. Ansmann, R. Neuber, P. Rairoux, U. Wandinger (Springer, Berlin Heidelberg 1997), pp. 423–426

Zhao, Y. Z., 1999: Signal-induced fluorescence in photomultipliers in differential absorption lidar systems. *Appl. Opt.*, **38**, 4639-4648.

Table 1: Summary of TOPAZ lidar specifications

Ozone concentration accuracy	Typically <5%, but can be as high as 15% under low signal-to-noise ratio conditions at ranges >2.5 km with high ozone concentrations
Ozone concentration precision	±2-5 ppbv (5-8%) at close ranges (400-500 m) and falls to ±5-35 ppbv (12-30%) at ranges >2.5 km with the largest uncertainties occurring under low SNR conditions as noted above
Resolution: ozone concentration	Vertical: 90 m (with 450 m smoothing) Horizontal (time): 600 m (10 s at a flight speed of 60 m/s)
Resolution: aerosol backscatter	Vertical: 18 m Horizontal (time): 600 m (10 s at a flight speed of 60 m/s)
Minimum, maximum range	400 m, 3000-5000 m
Laser specifications (per manufacturer) (See notes in text regarding operating at reduced output.) (All pulses at 1000 Hz)	1053 nm (18 mJ pulse <sup>-1</sup> ) 527 nm (11 mJ pulse <sup>-1</sup> ) 263 nm (2.8 mJ pulse <sup>-1</sup> ) 283-310 nm (≥ 0.2 mJ pulse <sup>-1</sup> with maximum of 0.8 mJ pulse <sup>-1</sup> at 290 nm)
Power requirement	3 kW of 110 VAC
Size (volume), weight laser frame chiller rack mounted electronics and computers  2x racks to hold electronics nitrogen cylinder	Approximately 1.75 m <sup>3</sup> , 400 kg total 1.4 m x 0.76 m x 1.2 m, 185 kg 0.70 m x 0.38 m x 0.59 m, 76 kg total of 1.4 m height of rack space needed for 0.48 m wide units (unit depths range from 0.05 m to 0.46 m), 83 kg 0.58 m x 0.51 m x 1.0 m, 16 kg each 0.2 m diameter, 0.7 m tall, 18 kg

## List of Figures

Figure 1: Cutaway view of Twin Otter fuselage showing typical installation of the TOPAZ system. The lidar frame including the laser (green), telescope and receiver optics (dark blue), and the FPGA/digitizer/preprocessing computer (magenta) is mounted on shock absorbing mounts (red) in the aft section of the cabin over the port in the underside of the fuselage. The remaining computers (magenta) and control electronics (cyan) are mounted in racks forward of the lidar. The laser chiller (orange) and a nitrogen gas cylinder (yellow) for the laser pressure control (and purge) system are mounted forward of the racks.

Figure 2: Schematic diagram of the TOPAZ lidar system. The numbers in parentheses on each computer refer to the order described in the text. Additional details of the components are given in the text.

Figure 3: Example of an offset and EMI corrected, blended TOPAZ lidar signal at 288.7 nm taken on 17 August 2006 during the TexAQS 2006. The figure shows the signal prior to SIB/overshoot correction (black), the exponential curve fitted to the tail of the signal (blue), and the corrected lidar signal after subtraction of the exponential fit function (red). All signals are averaged over 60 s. Signals are shown at full scale over the entire measurement range (a) and zoomed in on the region around the ground return (b), indicated by the black box in Figure 3a. The dotted line in Figure 3b indicates the

beginning of the fit range at 60 range gates or 360 m beyond the ground spike, which is visible at about 3400 m range.

Figure 4: Ozone (black) and SO<sub>2</sub> (red) absorption cross-sections over the usable tuning range of TOPAZ. Absorption cross sections are at 298 K after Burrows et al. (1999) for ozone and Vandaele et al. (2009) for SO<sub>2</sub>. The vertical lines indicate a set of TOPAZ wavelengths that may be used to measure ozone and SO<sub>2</sub> concentrations simultaneously.

Figure 5: Ozone cross-sections measured with the TOPAZ lidar downwind of the Houston metropolitan area. Cross sections extend vertically from near the surface to 2700 m MSL.

Figure 6: University of Houston ozonesonde launch site and Twin Otter flight path. The squares show the locations of the individual 10-s TOPAZ profiles. The dashed box encloses the three (filled) squares nearest the ozonesonde launched at 1829 UT. The dotted red line shows the path of the ozonesonde from the surface to 4000 m MSL.

Figure 7: Latitude-height curtain plot showing the TOPAZ and ozonesonde measurements at the locations plotted in Figure 6. The squares along the top again show the centers of the 10s lidar profiles. The three filled squares and dashed box show those profiles nearest the ozonesonde. The ozonesonde profile is color-coded to show the ozone concentration.

Figure 8: Mean and standard deviation (black) of the three TOPAZ profiles (gray) from Figure 7, plotted along with the ozonesonde profile in red.

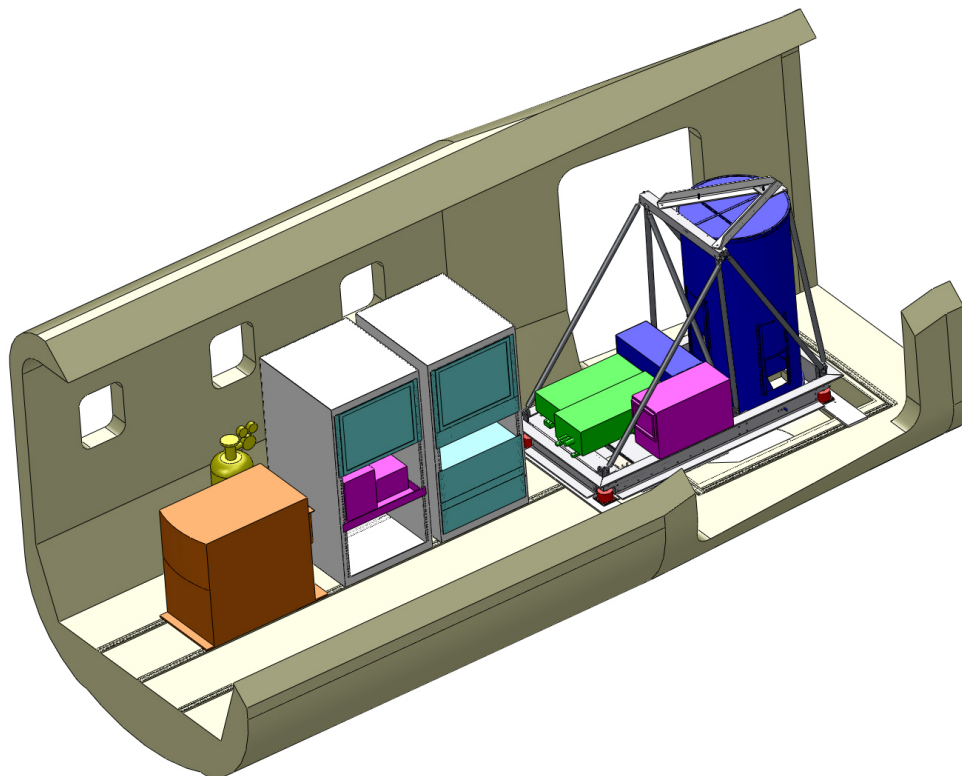


Figure 1: Cutaway view of Twin Otter fuselage showing typical installation of the TOPAZ system. The lidar frame including the laser (green), telescope and receiver optics (dark blue), and the FPGA/digitizer/preprocessing computer (magenta) is mounted on shock absorbing mounts (red) in the aft section of the cabin over the port in the underside of the fuselage. The remaining computers (magenta) and control electronics (cyan) are mounted in racks forward of the lidar. The laser chiller (orange) and a nitrogen gas cylinder (yellow) for the laser pressure control (and purge) system are mounted forward of the racks.

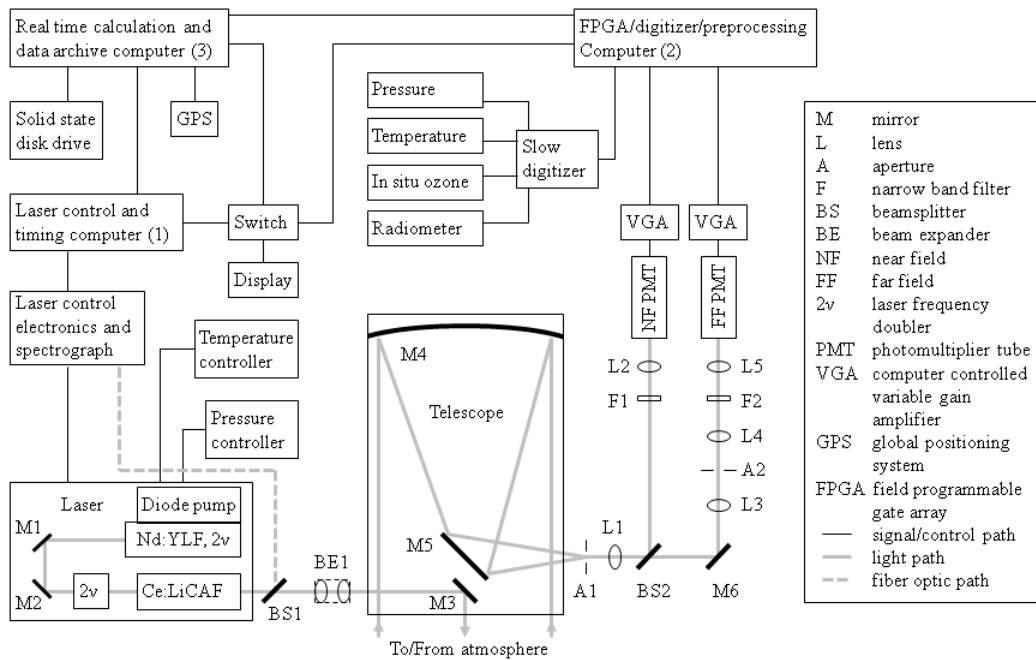


Figure 2: Schematic diagram of the TOPAZ lidar system. The numbers in parentheses on each computer refer to the order described in the text. Additional details of the components are given in the text.

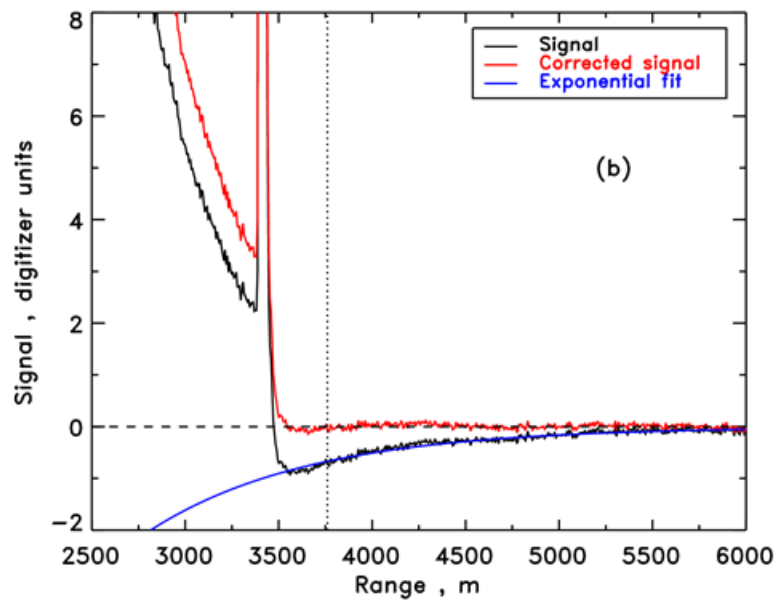
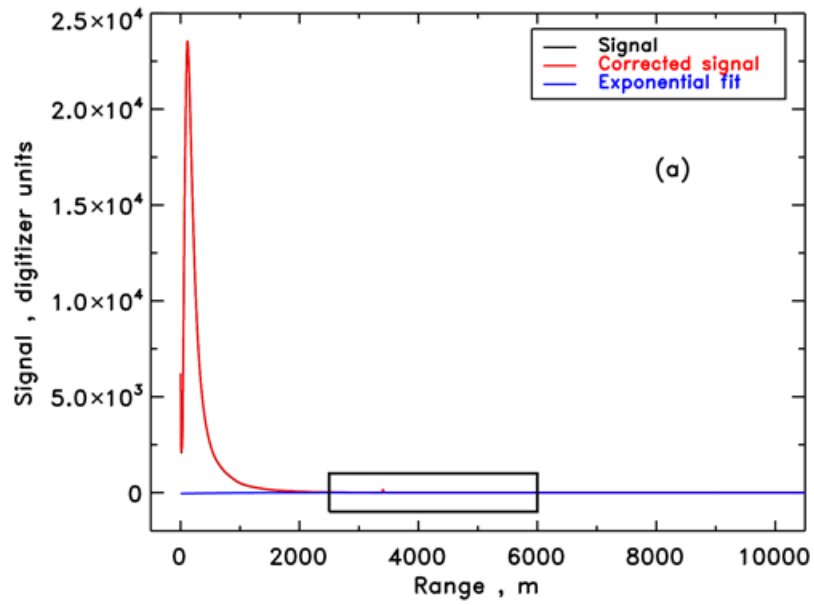


Figure 3: Example of an offset and EMI corrected, blended TOPAZ lidar signal at 288.7 nm taken on 17 August 2006 during the TexAQS 2006. The figure shows the signal prior to SIB/overshoot correction (black), the exponential curve fitted to the tail of the signal (blue), and the corrected lidar signal after subtraction of the exponential fit function (red). All signals are averaged over 60 s. Signals are shown at full scale over

the entire measurement range (a) and zoomed in on the region around the ground return (b), indicated by the black box in Figure 3a. The dotted line in Figure 3b indicates the beginning of the fit range at 60 range gates or 360 m beyond the ground spike, which is visible at about 3400 m range.

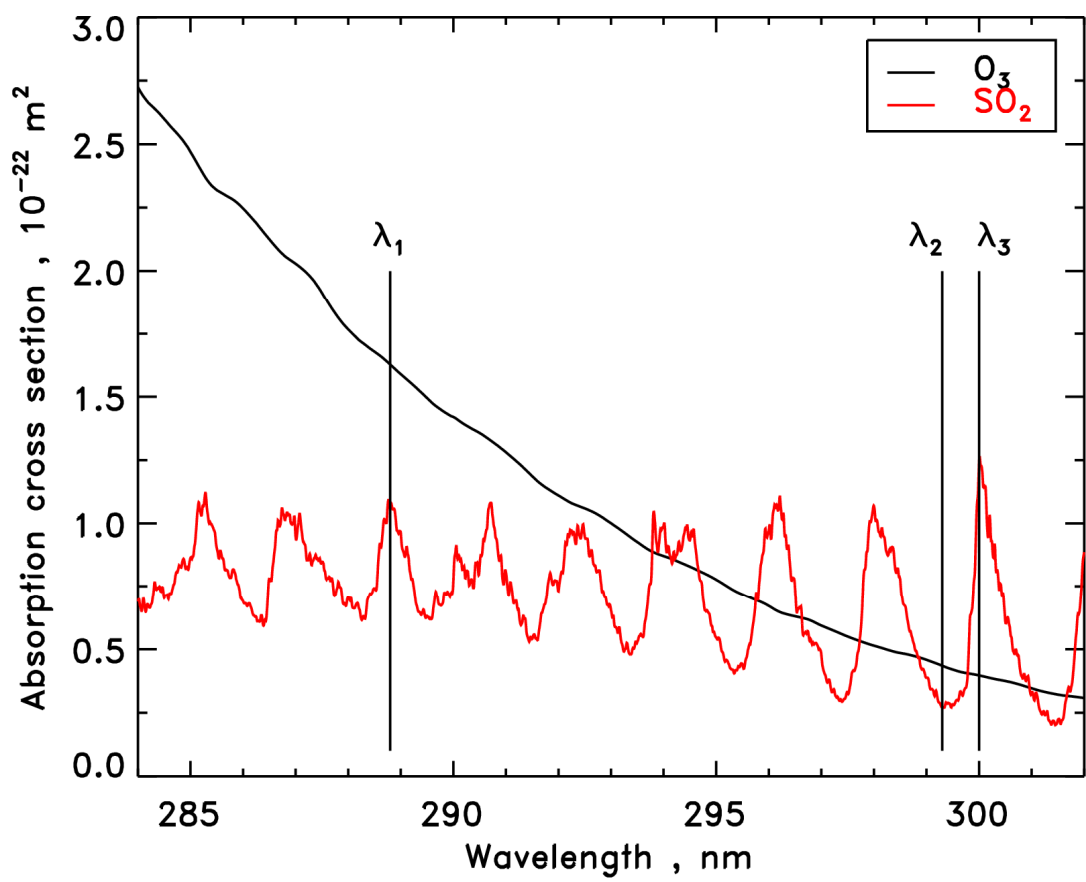


Figure 4: Ozone (black) and SO<sub>2</sub> (red) absorption cross-sections over the usable tuning range of TOPAZ. Absorption cross sections are at 298 K after Burrows et al. (1999) for ozone and Vandaele et al. (2009) for SO<sub>2</sub>. The vertical lines indicate a set of TOPAZ wavelengths that may be used to measure ozone and SO<sub>2</sub> concentrations simultaneously.

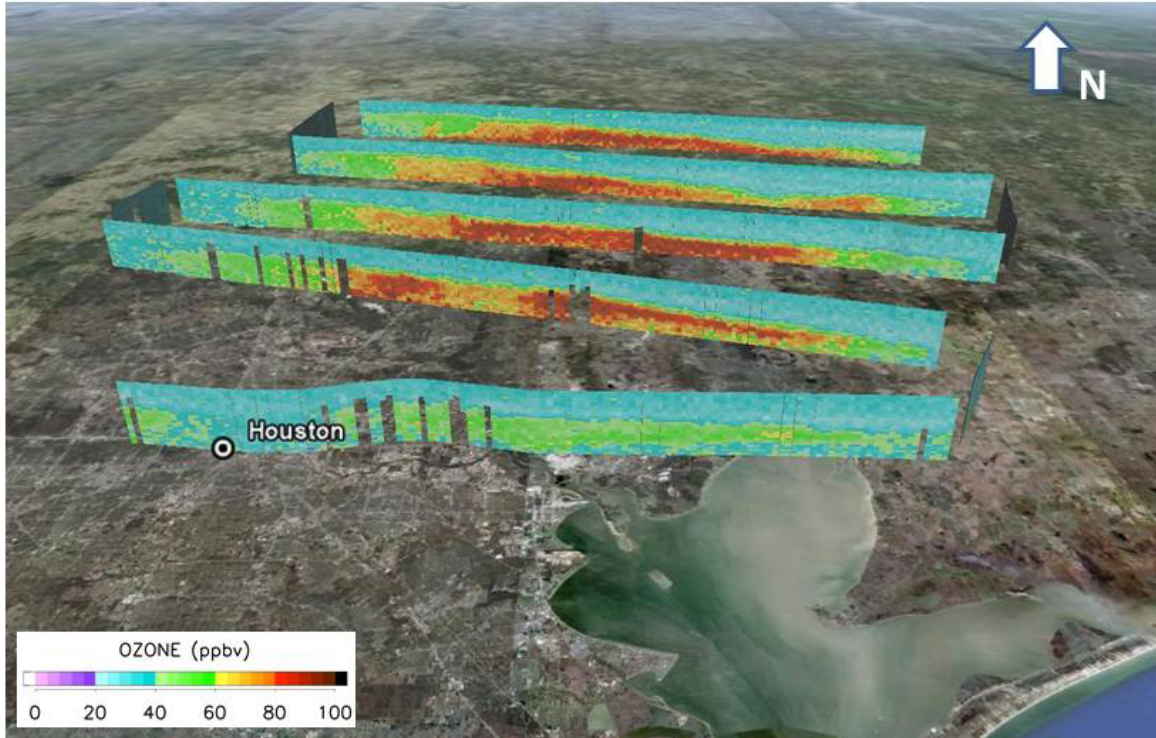


Figure 5: Ozone cross-sections measured with the TOPAZ lidar downwind of the Houston metropolitan area on 14 August 2006, 20:39 – 23:27 UT. Cross sections extend vertically from near the surface to 2700 m MSL. The TOPAZ measurements were made with the 286.0/297.3 nm wavelength pair.

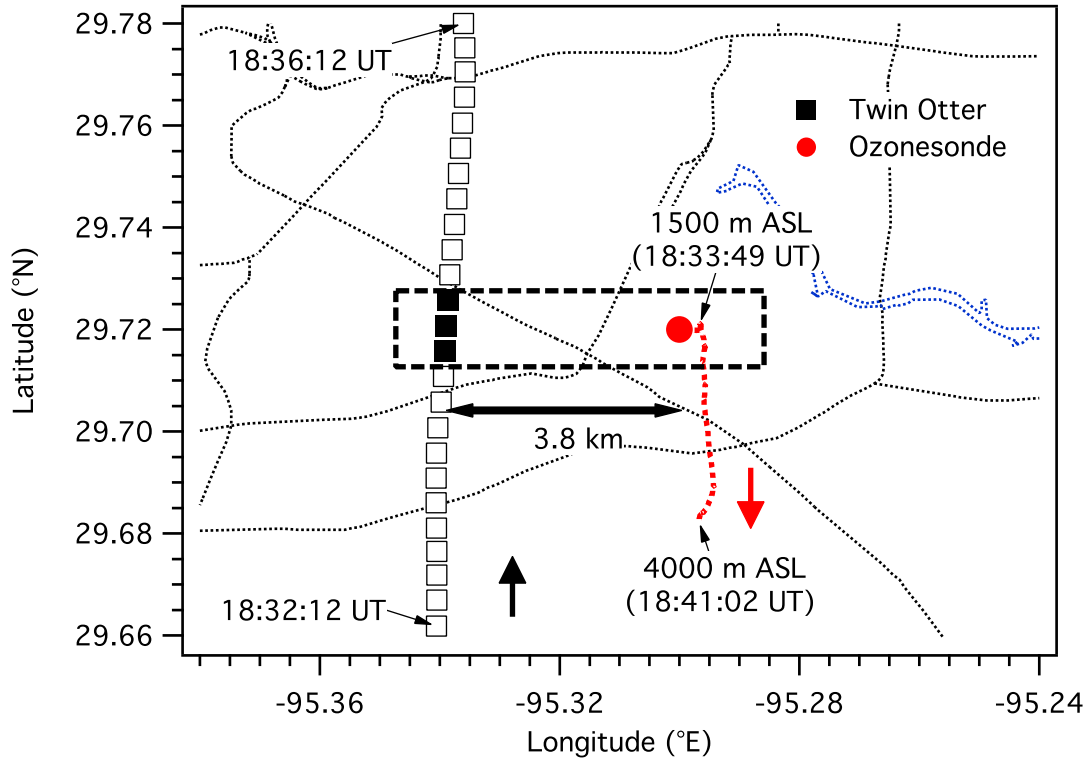


Figure 6: University of Houston ozonesonde launch site and Twin Otter flight path. The squares show the locations of the individual 10-s TOPAZ profiles. The dashed box encloses the three (filled) squares nearest the ozonesonde launched at 1829 UT. The dotted red line shows the path of the ozonesonde from the surface to 4000 m MSL.

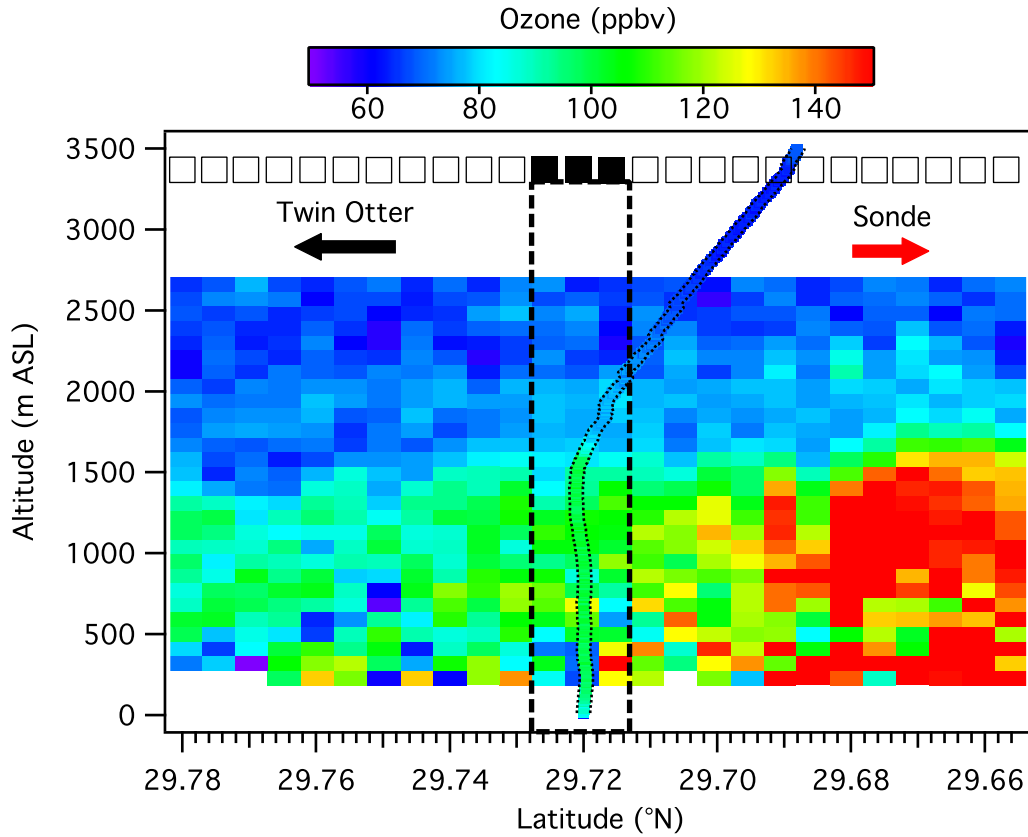


Figure 7: Latitude-height curtain plot showing the TOPAZ and ozonesonde measurements from 31 August 2006 at the locations plotted in Figure 6. The TOPAZ measurements were made with the 288.9/300.0 nm wavelength pair. The squares along the top again show the centers of the 10s lidar profiles. The three filled squares and dashed box show those profiles nearest the ozonesonde. The ozonesonde profile is color-coded to show the ozone concentration.

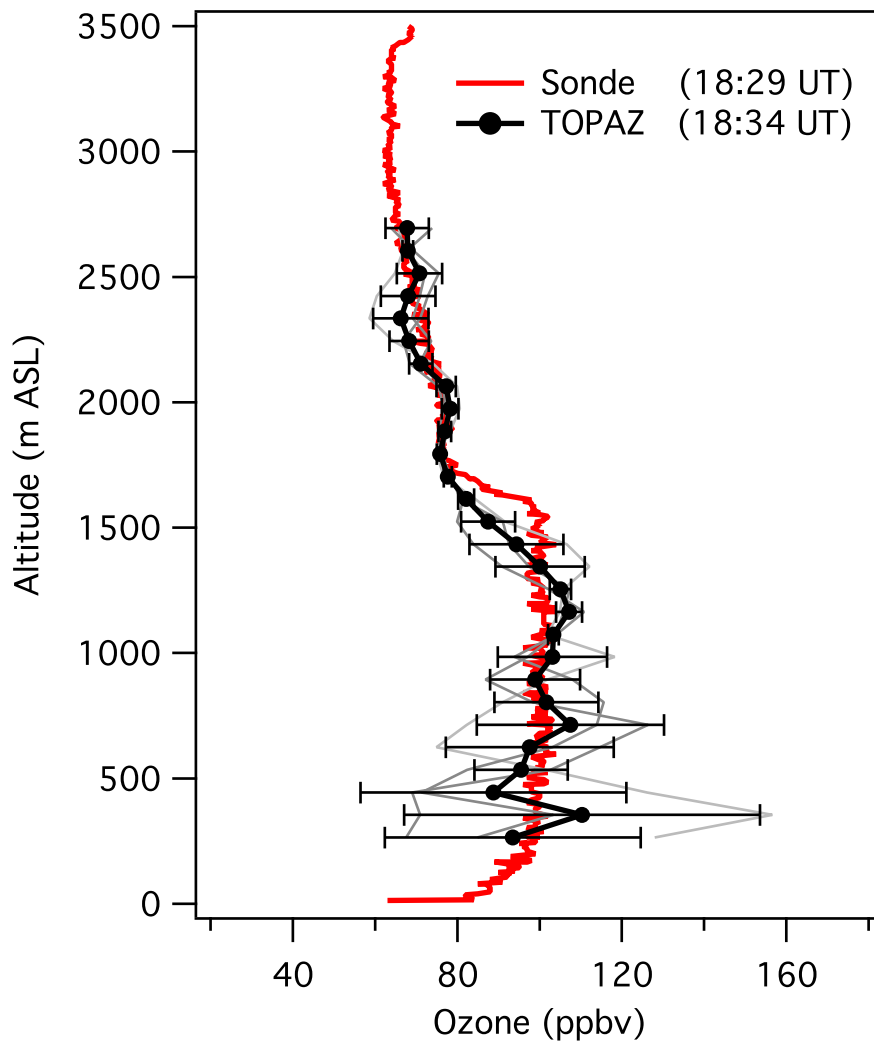


Figure 8: Mean and standard deviation (black) of the three TOPAZ profiles (gray) from Figure 7, plotted along with the ozonesonde profile in red.